Liquid−Liquid and Solid−Liquid Equilibria in Systems Containing *n*-Eicosane, *n*-Tetracosane, Ethanol, and Water

Kouji Maeda,† Ronald W. Rousseau, and Amyn S. Teja*

School of Chemical Engineering, Georgia Institute of Technology, Atlanta, Georgia 30332-0100

The partitioning of *n*-eicosane (C_{20}) and *n*-tetracosane (C_{24}) between a melt phase (L_1) and an aqueous ethanol phase (L_2) at 333.2 K, and between a solid phase (S) and an aqueous ethanol phase (L) at 293.2 K was measured. The wax content of aqueous ethanol solutions was greater when the solutions were in equilibrium with a melt wax phase (liquid−liquid equilibrium) than when they were in equilibrium with a solid wax phase (solid−liquid equilibrium). The distribution coefficients of C_{20} and C_{24} between the aqueous phase and a wax phase were also significantly higher in the case of liquid−liquid equilibrium than in the case of solid−liquid equilibrium. The data could be modeled satisfactorily using simple thermodynamic expressions based on the UNIFAC activity coefficient approach.

Introduction

The solubility of hydrophobic compounds, such as waxes, in aqueous solutions is of interest in a number of applications, including the recently proposed liquid membrane separation of waxes.[1] Unfortunately, phase equilibrium data relevant to these applications are not readily available in the literature. Two types of phase equilibria are of interest in these systems: (i) liquid−liquid equilibria between a melt wax phase (L_1) and an aqueous phase (L_2) at a relatively high temperature, and (ii) solid−liquid equilibria between a solid wax phase (S) and an aqueous phase (L) at a relatively low temperature.

An objective of this study was to compare the relative distribution of two hydrophobic solutes between an aqueous solution and a melt or solid phase comprised primarily of those solutes. *n*-Eicosane (C_{20}) and *n*-tetracosane (C_{24}) were chosen as the model solutes, and their solubilities in aqueous ethanol solutions were measured as a function of ethanol concentration. The data were correlated using simple thermodynamic models with activity coefficients calculated using the UNIFAC approach.[2] In addition, the binary phase diagram for $C_{20} + C_{24}$ mixtures was measured using differential scanning calorimetry (DSC).

Experimental Section

Materials. *n*-Eicosane and *n*-tetracosane were obtained from the Aldrich Company and had a stated purity greater than 99 mass %, with impurities that consisted mainly of isomeric alkanes. The purity was confirmed by gas chromatography, and the materials were used as received. High-purity ethanol (purity greater than 99.99 vol %) and deionized, ultrafiltered water were used to prepare aqueous ethanol solutions.

Procedures. Known masses (w_i) of *n*-eicosane (C_{20}), *n*-tetracosane (C_{24}), ethanol (E), and water (W) were mixed in a cell, and the cell was heated to 343.2 K in a water bath maintained at that temperature. The temperature of the contents of the cell was measured with a platinum resistance thermometer to an accuracy of ±0.1 K. Two liquid phases were obtained—a light phase (L_1) consisting mostly of C_{20} and C_{24} (the melt phase), and a dense phase (L_2) consisting mostly of water and ethanol with very small amounts of C_{20} and C_{24}. The partially miscible system was kept emulsified by slight shaking for several hours until equilibrium was achieved at a temperature of 333.2 K. The emulsion easily separated into two liquid phases after a further 2 h. A sample of the aqueous solution was then withdrawn with a syringe, placed in a glass dish, and dried for 2 weeks. The residual solid was weighed and dissolved in cyclohexane, and its composition was determined by GC analysis. The gas chromatograph was a Varian instrument (model 3700) with a packed column (Petrocol B, Supelco) and FID detector. The mole fractions x_W^{L2}, x_E^{L2}, x_{C20}^{L2}, and x_{C24}^{L2} of the components (W, E, C_{20}, and C_{24}) of the aqueous phase (L_2) were obtained from the initial mass measurements combined with the mass measurements of the dried solids and the GC analysis described above. The melt phase (L_1) was assumed to contain no water or ethanol and to consist of C_{20} and C_{24} in a ratio corresponding to the ratio of the initial amounts of each added to the system. Its composition was determined accordingly.

After determination of the L_1-L_2 equilibrium, the water bath temperature was lowered to 293.2 K, and the contents of the cell were kept at this temperature for 4 h until solid crystals deposited from the solution. Samples of the crystals were withdrawn and dried as described previously. The dried solid was weighed and dissolved in cyclohexane, and the mole fractions (x_{C20}^S, x_{C24}^S) in the solid phase (S) were determined by GC analysis. These compositions were close to the ethanol and water-free mole fractions of the two hydrocarbons in the solidified melt phase in the cell. Furthermore, it proved difficult to obtain a representative sample of the crystals. The compositions were therefore obtained from that of the solidified melt wax phase present in the cell. The mole fractions x_W^L, x_E^L, x_{C20}^L, and x_{C24}^L of the components in the aqueous ethanol phase (L) were obtained from mass measurements and GC analysis as described previously.

Each experiment was repeated three times, and average values of the solubilities are reported below. The uncer-

* Corresponding author. E-mail: amyn.teja@che.gatech.edu.
† Current address: Department of Chemical Engineering, Himeji Institute of Technology, 2167 Shosha, Himeji, Hyogo 671-2201, Japan.

10.1021/je015513f CCC: $22.00
Published on Web 12/20/2001

Table 1. Masses (w_i) and Mole Fractions (x^i) of Water (W), Ethanol (E), Eicosane (C_{20}), and Tetracosane (C_{24}) in the Initial Mixture

mass/g							
w_W	w_E	w_{C20}	w_{C24}	x^i_W	x^i_E	x^i_{C20}	x^i_{C24}
1.00	7.02	0.75	0.25	0.263	0.721	0.0125	0.0035
2.00	6.24	0.75	0.25	0.444	0.542	0.0106	0.0030
3.00	5.46	0.75	0.25	0.577	0.411	0.0092	0.0026
1.00	7.02	0.50	0.50	0.263	0.722	0.0084	0.0070
1.50	6.63	0.50	0.50	0.361	0.625	0.0077	0.0064
2.00	6.24	0.50	0.50	0.444	0.543	0.0071	0.0059
1.00	7.02	0.25	0.75	0.263	0.722	0.0042	0.0105
1.50	6.63	0.25	0.75	0.361	0.625	0.0038	0.0096
2.00	6.24	0.25	0.75	0.445	0.543	0.0035	0.0089

Table 2. Composition of the Aqueous Ethanol Phase (L_2) in Equilibrium with a Melt Wax Phase (L_1) at 333.2 K

x^{L1}_{C20}	x^{L1}_{C24}	x^{L2}_W	x^{L2}_E	x^{L2}_{C20}	x^{L2}_{C24}
0.781	0.219	0.267	0.732	0.001 180	0.000 126
0.779	0.221	0.450	0.550	0.000 176	0.000 014
0.780	0.220	0.584	0.416	0.000 042	0.000 003
0.545	0.455	0.267	0.732	0.000 842	0.000 296
0.546	0.454	0.366	0.634	0.000 399	0.000 126
0.546	0.454	0.450	0.550	0.000 129	0.000 038
0.286	0.714	0.267	0.732	0.000 472	0.000 539
0.284	0.716	0.366	0.634	0.000 200	0.000 187
0.282	0.718	0.450	0.550	0.000 077	0.000 000

tainties in the mole fractions of water and ethanol were estimated to be ±1%, and those in the mole fractions of C_{20} and C_{24} in the melt (L_1) and solid phases (S) were also estimated to be ±1%. These mole fractions were obtained via mass measurements. On the other hand, the uncertainties in the mole fractions of C_{20} and C_{24} in the aqueous phases (L_2 and L) were estimated to be ±10%, as these mole fractions were obtained via GC analysis of dried samples.

DSC Experiments. A small amount (5 to 10 mg) of a binary mixture of C_{20} and C_{24} (mole fraction x°_{C20}) was placed on one of two aluminum pans in a Setaram DSC (model DSC-TG-111), and both pans were heated by nitrogen flowing at 50 mL/min. The heating program ranged from 293 K to 343 K, and the temperature of the sample was scanned at three different heating rates (2 K/min, 3 K/min, and 5 K/min). Peak and onset temperatures on each DSC scan were identified as a function of the heating rate; these values are taken to be estimates of the point at which the last and first of the solid sample melts, respectively. Final estimates of the liquidus (peak) temprature T_L and solidus (onset) temperature T_S were obtained by extrapolating the results from the different heating rates to a heating rate of 0 K/min.

Results

L_1−L_2 Equilibria at 333.2 K. The amounts of each species added to the system and the resulting composition of the initial mixture are shown in Table 1. The compositions of the melt (L_1) and aqueous ethanol (L_2) phases in equilibrium are shown in Table 2. Figure 1 shows the expected result that the total wax fraction ($=x^{L2}_{C20} + x^{L2}_{C24}$) in the aqueous ethanol solution increases with an increase in the ethanol mole fraction in the solution. In addition, the total wax fraction was found to be slightly higher when the melt contained more of the lower molecular weight *n*-alkane C_{20}. Figure 2 is a plot of the distribution coefficients K^{LL}_{C20} ($=x^{L2}_{C20}/x^{L1}_{C20}$) and K^{LL}_{C24} ($=x^{L2}_{C24}/x^{L1}_{C24}$) as functions of the ethanol mole fraction in the aqueous solution. The distribution coefficients exhibit an approximately linear

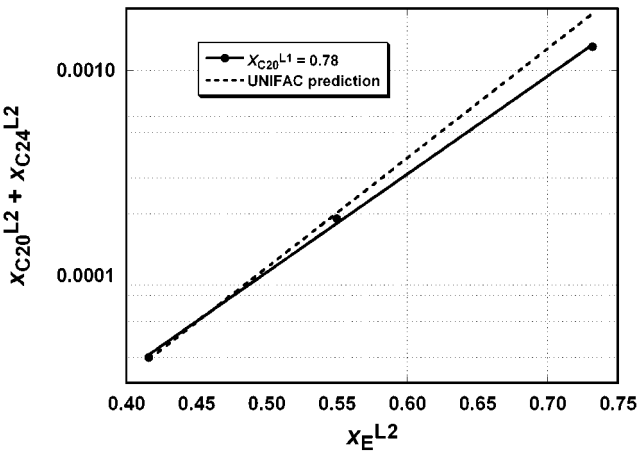

Figure 1. Total wax fraction in aqueous ethanol solutions at 333.2 K.

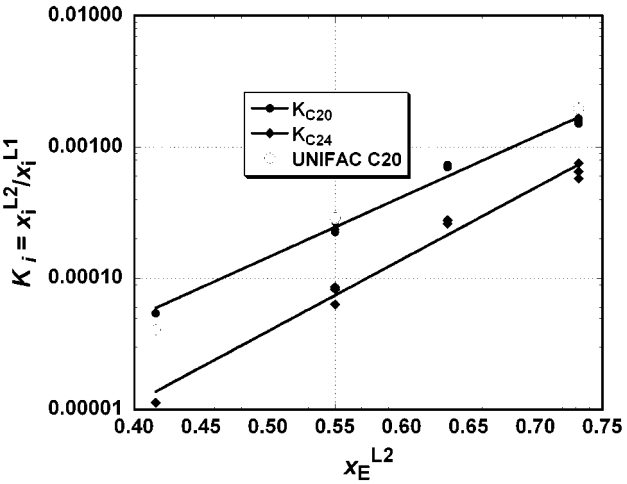

Figure 2. Distribution of C_{20} and C_{24} between melt and aqueous phases at 333.2 K.

Table 3. Composition of the Aqueous Ethanol Phase (L) in Equilibrium with a Solid Wax Phase (S) at 293.2 K

x^S_{C20}	x^S_{C20}	x^L_W	x^L_E	x^L_{C20}	x^L_{C24}
0.781	0.219	0.267	0.733	0.000 235	0.000 014 5
0.779	0.221	0.450	0.550	0.000 074	0.000 003 7
0.780	0.220	0.584	0.416	0.000 029	0.000 000 3
0.545	0.455	0.267	0.733	0.000 216	0.000 014 7
0.546	0.454	0.366	0.634	0.000 114	0.000 007 0
0.546	0.454	0.450	0.550	0.000 055	0.000 002 5
0.286	0.714	0.267	0.733	0.000 176	0.000 017 0
0.284	0.716	0.366	0.634	0.000 041	0.000 003 1
0.282	0.718	0.450	0.550	0.000 014	0.000 000 8

dependence with the ethanol content and a negligible dependence on the composition of the melt.

S−L Equilibria at 293.2 K. Compositions in the aqueous ethanol phase (L) in equilibrium with a solid wax phase (S) at 293.2 K are listed in Table 3. As shown in Figure 3, the total solubility of waxes ($=x^L_{C20} + x^L_{C24}$) in the aqueous ethanol phase was found to be a function of both the ethanol mole fraction and the ratio of C_{20} to C_{24} in the solid. The dependence on the latter variable was found to be greater than that in the corresponding LLE case. However, the distribution coefficients K^{SL}_{C20} ($=x^L_{C20}/x^S_{C20}$) and K^{SL}_{C24} ($=x^L_{C24}/x_{C24}{}^S$) showed substantially more scatter than that in the corresponding LLE system (as shown in Figure 4). We suspect that this scatter is related to the uncertainty associated with the formation of a uniform

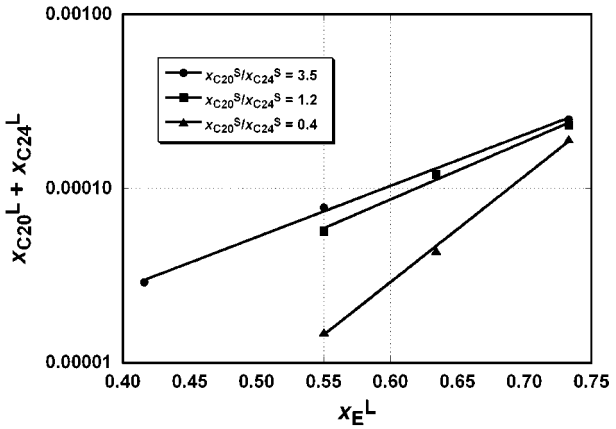

Figure 3. Total wax fraction in aqueous ethanol solutions at 293.2 K.

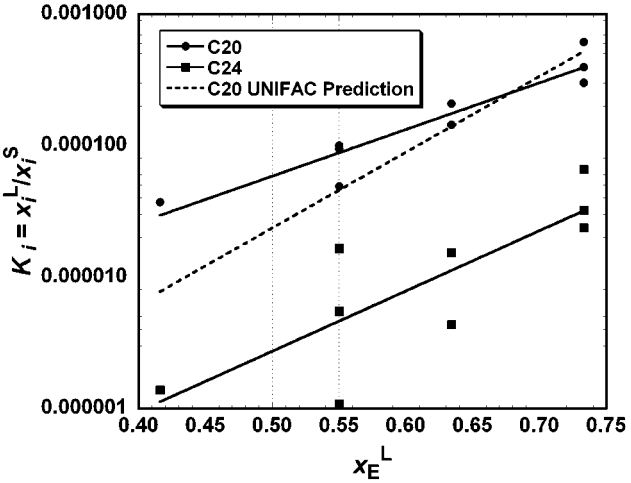

Figure 4. Distribution of C_{20} and C_{24} between solid and aqueous phases at 293.2 K.

Table 4. Onset and Peak Temperatures on DSC Curves

heating rate/K min^{-1}	onset temp, T_S/K	peak temp, T_L/K
	$x_{C20}^0 = 0.958$	
2.0	309.07	309.93
3.0	308.40	309.50
5.0	307.10	308.50
	$x_{C20}^0 = 0.737$	
2.0	309.80	312.32
3.0	309.09	311.88
5.0	308.16	311.18
	$x_{C20}^0 = 0.545$	
2.0	312.01	314.88
3.0	311.42	314.62
5.0	311.31	314.49
	$x_{C20}^0 = 0.339$	
2.0	314.63	318.78
3.0	314.08	318.30
5.0	312.72	317.19
	$x_{C20}^0 = 0.059$	
2.0	321.80	323.20
3.0	321.25	322.75
5.0	319.82	321.72

solid phase from a mixture of the melt and aqueous solution.

Binary Solid−Liquid Equilibrium. Table 4 lists the peak and onset temperatures from DSC curves for five different compositions of waxes at three different heating rates. These data were extrapolated to a heating rate of 0 K/min to estimate values of the liquidus and solidus temperatures. These extrapolated values were then used to construct the plot in Figure 5, which also shows curves generated assuming ideal solution behavior. Quantitative data on pure-component solid-phase transition temperatures could not be obtained because of the limited temperature range of the DSC apparatus. However, pure C_{20} does not exhibit a solid-phase transition, whereas the transition temperature for C_{24} has been reported in the literature and is given along with other pure-component properties[3,4] in Table 5.

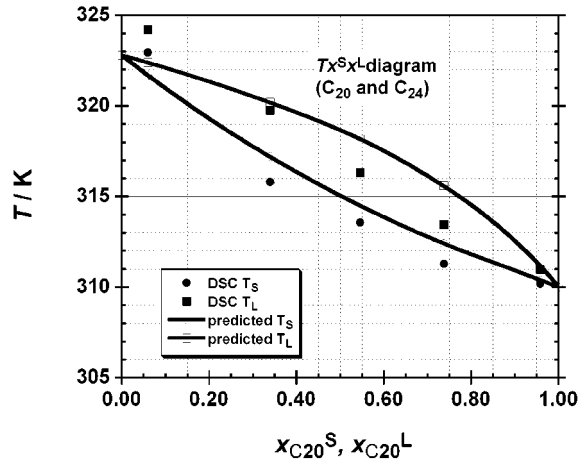

Figure 5. Solid−liquid equilibria in the binary C_{20} + C_{24} system.

Table 5. Physical Properties of *n*-Eicosane and *n*-Tetracosane[3,4,6] Used in Calculations

	T^m/K	ΔH^m/J mol^{-1}	T^t/K	ΔH^t/J mol^{-1}
C_{20}	310.0	69 880		
C_{24}	323.75	54 840	321.25	31 270

Modeling. For liquid−liquid equilibrium between the melt phase (L_1) and the aqueous ethanol phase (L_2), we may write

$$x_i^{L1}\gamma_i^{L1} = x_i^{L2}\gamma_i^{L2} \qquad i = C_{20}, C_{24}, E, W \qquad (1)$$

Here γ_ι represents the activity coefficient of component i in the phase denoted by the superscript. We have assumed that the temperature is fixed and the ratios of C_{20} to C_{24} in the melt phase (L_1) and of ethanol to water in the aqueous phase (L_2) are the same as those in the initial mixture; that is, $x_{C20}^{L1}/x_{C24}^{L1} \approx x_{C20}^{i}/x_{C24}^{i}$ and $x_E^{L2}/x_W^{L2} \approx x_E^{i}/x_W^{i}$. These quantities are known from their initial compositions (Table 1). Moreover, the sum of the mole fractions of the components must be unity in each phase. This leaves four unknowns (x_E^{L1}, x_{C24}^{L1}, x_E^{L2}, and x_{C24}^{L2}) and four equations. The equations may therefore be solved for these unknowns provided an activity coefficient model is available.

Activity coefficients were obtained using UNIFAC parameters for LLE reported by Magnussen et al.[5] Predicted wax content and distribution coefficients were in reasonably good agreement with experiment, as shown in Figures 1 and 2.

Equation 1 can be rearranged to solve for the distribution coefficient as follows:

$$K_{C20}^{LL} = \frac{x_{C20}^{L2}}{x_{C20}^{L1}} = \frac{\gamma_{C20}^{L1}}{\gamma_{C20}^{L2}} \qquad (2)$$

Moreover, since the melt phase is essentially a solution of two long-chain hydrocarbons and can be assumed to be

ideal, $\gamma_{C20}^{L1} \rightarrow 1.0$, and therefore

$$K_{C20}^{LL} = \frac{x_{C20}^{L2}}{x_{C20}^{L1}} = \frac{1}{\gamma_{C20}^{L2}} \tag{3}$$

The distribution coefficient therefore depends only on the composition of the aqueous phase, as can be seen in Figure 2.

For equilibrium between a solid wax phase (S) and an aqueous phase (L), we may write

$$x_{C20}^{S}\,\gamma_{C20}^{S}\,f_{C20}^{S} = x_{C20}^{L}\,\gamma_{C20}^{L}\,f_{C20}^{L} \tag{4}$$

$$x_{C24}^{S}\,\gamma_{C24}^{S}\,f_{C24}^{S} = x_{C24}^{L}\,\gamma_{C24}^{L}\,f_{C24}^{L} \tag{5}$$

Here f_i^L is the fugacity of component i in the liquid phase L, f_i^S is the fugacity of component i in the solid phase S, and the other variables have been defined previously. We may assume that only the waxes partition between the two phases, and the solid phase contains no water or ethanol. We may also assume that the solid phase behaves ideally (since it is essentially a solution of two long-chain hydrocarbons). Finally, the standard-state fugacity ratio may be obtained from well-known thermodynamic expressions,[6] so that

$$R\,\ln(x_{C20}^{L}\,\gamma_{C20}^{L}/x_{C20}^{S}) = \Delta H_{C20}^{m}\left(\frac{1}{T_{C20}^{m}} - \frac{1}{T}\right) \tag{6}$$

$$R\,\ln(x_{C24}^{L}\,\gamma_{C24}^{L}/x_{C24}^{S}) = \Delta H_{C24}^{m}\left(\frac{1}{T_{C24}^{m}} - \frac{1}{T}\right) + \Delta H_{C24}^{t}\left(\frac{1}{T_{C24}^{t}} - \frac{1}{T}\right) \tag{7}$$

ΔH^m and T^m are the enthalpy of fusion and melting temperature, respectively, whereas ΔH^t and T^t are the enthalpy of the solid-phase transition and the transition temperature. C_{20} does not exhibit a solid-phase transition, and this is reflected in eq 6. Solubilities at 293.2 K were calculated by solving eqs 6 and 7 using the UNIFAC model to obtain activity coefficients and the properties of C_{20} and C_{24} listed in Table 5. The total wax content and distribution coefficients were reasonably well predicted, as shown in Figures 3 and 4. This approach, therefore, represents an excellent first approximation to the prediction of L−L and S−L equilibria in the system studied.

Binary S−L behavior involving only C_{20} and C_{24} can be predicted from eqs 6 and 7 by assuming that the activity coefficients in both the solid and liquid (melt) phases approach 1.0, since both phases are now solutions of two long-chain hydrocarbons. Under such circumstances

$$R\,\ln(x_{C20}^{L}/x_{C20}^{S}) = \Delta H_{C20}^{m}\left(\frac{1}{T_{C20}^{m}} - \frac{1}{T}\right) \tag{8}$$

and

$$R\,\ln(x_{C24}^{L}/x_{C24}^{S}) = \Delta H_{C24}^{m}\left(\frac{1}{T_{C24}^{m}} - \frac{1}{T}\right) + \Delta H_{C24}^{t}\left(\frac{1}{T_{C24}^{t}} - \frac{1}{T}\right) \tag{9}$$

Predictions from these equations are shown along with the DSC data in Figure 5. Again, the predictions compare reasonably well with the measurements, although agreement is by no means exact.

It is not the intent of this work to recommend simple predictive models for all cases in which hydrophobic solutes partition between nonpolar and aqueous phases. The above development has been undertaken to demonstrate that simple models represent useful starting points for the correlation and prediction of phase equilibria in these systems.

Conclusions

Liquid−liquid and solid−liquid equilibria in a system containing *n*-eicosane, *n*-tetracosane, ethanol, and water were measured in this work. In addition, the binary solid−liquid behavior of *n*-eicosane and *n*-tetracosane mixtures was obtained from DSC measurements. The wax content of aqueous ethanol solutions was greater when the solutions were in equilibrium with a melt phase (L−L equilibria) than when they were in equilibrium with a solid phase (S−L equilibria). Moreover, the distribution coefficients of the waxes were larger in the L−L equilibrium case than in the case of S−L equilibria. This allows a liquid membrane separation process to be designed for the separation of the two hydrocarbons, as discussed by Maeda and Rousseau.[1] Liquid−liquid equilibria could be predicted satisfactorily using the UNIFAC activity coefficient model. However, the predictions were less satisfactory in the case of solid−liquid equilibria.

Literature Cited

Maeda, K.; Rousseau, R. W. Separation of Waxes by Liquid-Membrane Mediated Crystallization. *Proceedings of the 14th International Symposium on Industrial Crystallization*, Cambridge, 1999; Institution of Chemical Engineers: Rugby, U.K., 1999; pp 1680−1687.

Fredenslund, A.; Jones, R. L.; Prausnitz, J. M. Group-Contribution Estimation of Activity Coefficients in Nonideal Liquid Mixtures. *AIChE J.* **1975**, *21*, 1086−1099.

Mozes, G. Y. *Paraffin Products*; Elsevier: Amsterdam, 1982.

Reid, R. C.; Prausnitz, J. M.; Poling, B. E. *The Properties of Gases and Liquids*, 4th ed.; McGraw-Hill: New York, 1986.

Magnussen, T.; Rasmussen, P.; Fredenslund, A. UNIFAC Parameter Table for Prediction of Liquid−Liquid Equilibria. *Ind. End. Chem. Process Des. Dev.* **1981**, *20*, 331−339.

Roberts, K. L.; Rousseau, R. W.; Teja, A. S. Solubility of long-chain alkanes in heptane between 280 K and 350 K. *J. Chem. Eng. Data* **1994**, *39*, 793−795.

Received for review August 31, 2001. Accepted November 11, 2001.

JE015513F